ISBN: 978-3-95450-240-0 ISSN: 2673-5547 doi:10.18429/JACoW-HIAT2022-TUP17

BEAM DYNAMICS AND SPACE CHARGE STUDIES FOR THE INNOVATRON CYCLOTRON*

G. D'Agostino†, W. Kleeven
Ion Beam Applications (IBA), Louvain-La-Neuve, Belgium

Abstract

At IBA a high-intensity compact self-extracting cyclotron is being studied. There is no dedicated extraction device but instead, a special shaping of the magnetic iron and the use of harmonic coils to create large turn-separation. Proton currents up to 5 mA are aimed for. This would open new ways for large-scale production of medical radioisotopes. The main features of the cyclotron are presented. A major variable of the beam simulations is the space charge effect in the cyclotron centre. Using the SCALA-solver of Opera3D, we attempt to find the ion source plasma meniscus and the beam phase space and current extracted from it. With these properties known, we study the bunch formation and acceleration under high space charge condition with our in-house tracking code AOC. We also discuss a new tool that automatizes optimization of cyclotron settings for maximizing beam properties such as extraction efficiency.

INTRODUCTION

Radioisotopes for nuclear medicine can be produced either by reactors or accelerators. Commercial cyclotrons (E = 15–70 MeV) achieve currents up to or just above 1 mA. Large-scale production of radioisotopes needs a high-intensity cyclotron technology. The self-extracting cyclotron is a promising tool for producing high quantities of SPECT radioisotopes such as Tc-99m or new emerging PET radioisotopes [1]. The InnovaTron 14 MeV H^+ machine features a magnetic field with a very steep fall-off near the outer pole radius, allowing the beam to extract spontaneously. First harmonic coils increase the turn-separation at the entrance of the extraction path. The prototype, installed in Fleurus (Belgium) in 2000, achieved a current close to 2 mA [2]. More details on the concept can be found in [3]. Main goals set for the project are: i) improvement and optimization of the magnet, extraction elements and central region, ii) space charge simulations, iii) improvement of turn-separation at extraction. We discuss results obtained for i) and ii).

MAGNET OPTIMIZATION

The following improvements have been implemented as compared to the prototype: i) the magnet (and also the accelerating structure) has perfect 2-fold symmetry. This allows irradiation of two targets stations at opposite exit ports and to place two internal ion sources. The latter will increase cyclotron reliability and uptime, ii) the groove in the extraction path used in the prototype (Fig. 1a) is replaced by a "plateau" (Fig. 1b). This reduces the strong sextupole component in the extraction path and improves the extracted beam quality, iii) the pole gaps still have a quasi-elliptical shape, decreasing towards larger radii, but the iso-gap contours follow equilibrium orbits. This enables a steeper transition from the internal stable orbit towards the non-stable extracted orbit.

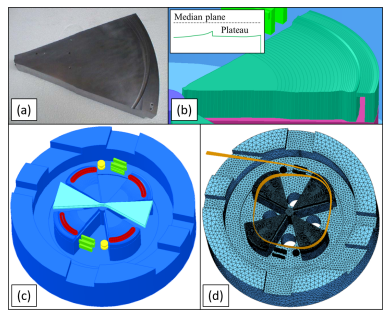

Figure 1: InnovaTron improved magnet design.

Figure 1c shows a view on the lower half of the magnet developed in Opera3D. The harmonic coils (in red) and the dees (in light blue) are also shown. The gradient correctors (in green) provide radial focusing to the extracted beam. The beam separators (in yellow) are used to intercept parts of the beam that are not properly extracted. A beam simulation of the last 5 turns superimposed on the FEM model is shown in Fig. 1d. Automatic and parametrized FEM models have been developed, for the magnet but also for the central region and dees. More details are given in [4].

CENTRAL REGION STUDIES

We do an effort for a self-consistent simulation of the space charge dominated beam in the central region. This method consists of three steps. In the first step the SCALA space charge solver of Opera3D [5] is used to find the plasma meniscus of the ion source. In the second step the same central region model is solved again, but now with the TOSCA electrostatic solver of Opera3D. Here the meniscus surface is put at ground potential. This provides the 3D electric field map everywhere in the central region, including the source-puller gap. In a third step the beam extracted from the meniscus is simulated in the 3D field map using the self-consistent in-house space-charge code AOC [6]. This code has been extended to also simulate the bunch formation process in the first gap.

SCALA Simulations

The plasma-free boundary module of SCALA calculates the plasma meniscus and the extracted beam phase space and current density on the meniscus, in a DC electric field.

* Work supported by the European Union's Horizon 2020 research and innovation programme under the Marie Skłodowska-Curie grant agreement No 886190.
† grazia.dagostino@iba-group.com

ISBN: 978-3-95450-240-0 ISSN: 2673-5547 doi:10.18429/JACoW-HIAT2022-TUP17

SCALA does not solve the plasma itself: the meniscus surface is determined by the Child-Langmuir condition where the external electric field on the surface is cancelled by the space charge electric field. The surface is found in an iterative process. The electric field in a cyclotron central region is not DC but RF. The RF frequency however, is so high that it will be impossible for the plasma meniscus to follow it, in its motion. The maximum velocity of a material wave is roughly equal to the speed of sound in the material which, for a plasma, will be close to the Bohm-velocity $v_B = \sqrt{kT_e/m_p}$, where T_e is the plasma electron temperature and m_p is the proton mass. Assuming $kT_e \approx 10$ eV we find that the meniscus could move only about 0.1 mm in a quarter of the wave period at 70 MHz. So it seems that the meniscus will move only weakly in the RF electric field; we therefore make the assumption that the meniscus shape and position can be found by solving the problem for the rms-value of the gap-voltage. It is clear that this is a strong assumption and an important simplification which we can, at this point not further validate.

For the solution of the SCALA problem we only need to model the local geometry of the source-puller gap. Our example is shown in Fig. 2. In this geometry the puller (C) and the dee (E) are placed at high (negative) potential and the chimney (A) and the dummy-dee (D) are at ground potential. The ion source full slit aperture in our example is

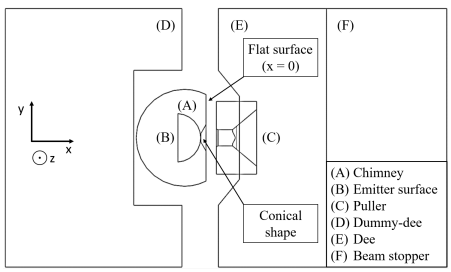

Figure 2: Top view of the SCALA source-puller model.

$\Delta y \times \Delta z = 1 \times 8\,\text{mm}^2$. SCALA lauches beamlets from the (flat) emitter surface (B), which move to the right towards the ion source slit. At this position, space charge builts up which limits the flow of extracted particles. Besides the geometry, the two important parameters in the simulation are i) the dee-voltage V_{dee} and ii) the emitter current density J_{emit}. Two additional but less critical parameters are iii) the electron temperature T_e and iv) the meniscus voltage V_m.

Figure 3 shows examples of four different cases: a) (V_{dee}=42.1 kV, $J_{emit} = 0.4\,\text{A/cm}^2$), b) V_{dee}=9.5 kV, $J_{emit} = 0.4\,\text{A/cm}^2$), c) ($V_{dee}$=38.9 kV, $J_{emit} = 0.2\,\text{A/cm}^2$) and d) ($V_{dee}$=38.9 kV, $J_{emit} = 2\,\text{A/cm}^2$). The first column in the figure is a vertical section through the chimney and shows the position and shape of the meniscus (only the upper half is shown). The middle column shows the vertical beam profile (seen from the $-y$ direction) and the right column shows the horizontal beam profile (seen from the $+z$ direction). The extracted DC currents for the four cases are 100 mA (a), 36.7 mA (b), 67.4 mA (c) and 222 mA (d).

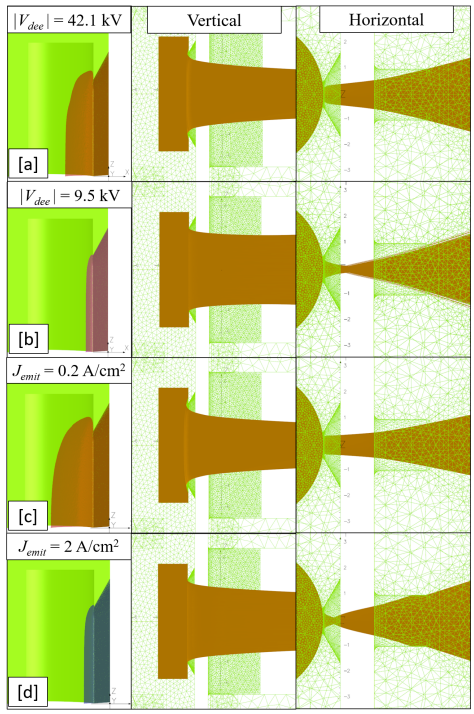

Figure 3: Examples of meniscus shape and beam projections.

A close inspection shows that the extracted current is (almost perfectly) proportional to the surface of the meniscus times the emitter current density. The beamlets cross the meniscus (almost perfectly) perpendicularly and the flow is (almost perfectly) laminar. It is seen that higher V_{dee} pushes the meniscus to the left and higher J_{emit} pushes the meniscus to the right. Horizontally the beam is strongly converging, with an (over-) focus close to the slit and vertically the beam is weakly converging. This relates directly to the slit dimensions which make that the meniscus is strongly curved in the xy-plane and much more flat in the xz-plane.

Figure 4 shows the extracted current and meniscus position as function of the four parameters V_{dee}, J_{emit}, T_e and V_m. The position is the distance between the extreme meniscus x-coordinate and the intersect between x-axis and plasma chamber cylinder.

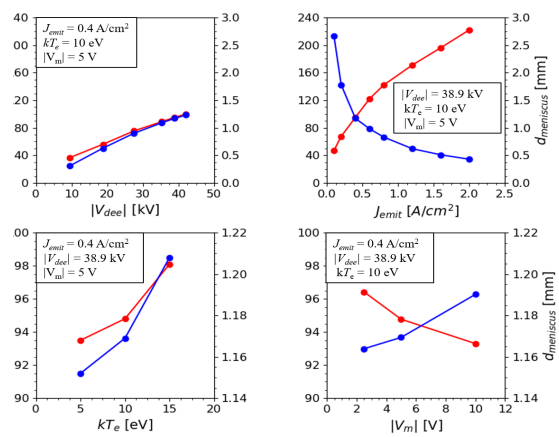

Figure 4: DC extracted current (red) and meniscus position (blue) as function of the four main parameters.

ISBN: 978-3-95450-240-0 ISSN: 2673-5547 doi:10.18429/JACoW-HIAT2022-TUP17

TOSCA Simulations

We extract from the beamlets calculated by SCALA (those who are extracted from the ion source), the particle position coordinates, the velocity components and the beamlet current at the meniscus intersect. These data are used to fit the meniscus x-coordinate, the transverse divergencies (y', z') and the beamlet currents as a function of y and z. The latter two are considered as independent variables. We use a double polynomial fit up to order 7 (the sum of the y and z exponents) and take into account the symmetry: x is even in y and z; y' is odd in y and even in z; z' is even in y and odd z. This allows to represent the surface of the meniscus as a wire-edge structure with a triangular mesh. This surface is included in the TOSCA model of the central region, where it is put at ground potential (see Fig. 5). With this, one can simulate precisely the value and shape of the 3D electric field in the source puller gap. The representation also allows to create a file with particle starting conditions for tracking, when y and z are generated randomly and the other variables (x, y', z') are calculated from the fits. Figure 6 shows projections of the fitted phase space on the planes xy, xz, yy' and zz'. There are three cases shown: $V_{dee} = 38.9$ kV, $J_{emit} = 0.4$ A/cm^2 (green), $V_{dee} = 18.8$ kV, $J_{emit} = 0.4$ A/cm^2 (blue), $V_{dee} = 38.9$ kV, $J_{emit} = 2$ A/cm^2 (red).

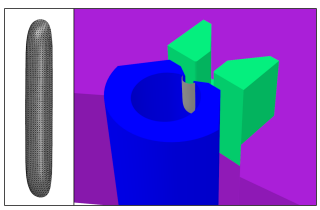

Figure 5: Modeling of the plasma meniscus in TOSCA.

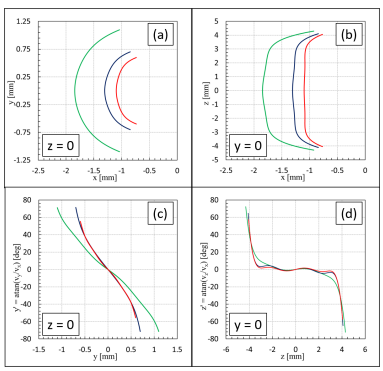

Figure 6: Fitted phase space projections.

Figure 7 shows in (a) the TOSCA electric field in the source-puller gap for three different cases. One case is for the chimney with the conical shape as shown in Fig. 2; for the other two cases this cone is not present. The meniscus was calculated at $V_{dee} = 35.3$ kV for the first case (green curve) and 18.8 kV for the other two cases. For all three cases, the electric field drops quickly in the space in between the meniscus and the chimney slit $(x < x_{slit})$. As a consequence, the particles must leave early from the meniscus surface in order to be able to cross the gap. This is illustrated in Figs. 7(b-d). They show the particle energy gain as a function of time for different starting RF phases ranging from -180° (the moment of zero dee-voltage) up to -130° in steps of 5° (with $V_{dee} = 55$ kV). Later starting phases are not properly accelerated by the central region. The worst case is (b) where the energy gain is the lowest and the energy spread is the largest. For this case, the electric field near the meniscus is the lowest and the particles are lost after a few turns in the central region. For cases (c) and (d) the electric field near the meniscus is higher and a phase range of about 40° can be accepted and accelerated. Case c is the best as it has good energy gain and the smallest energy spread.

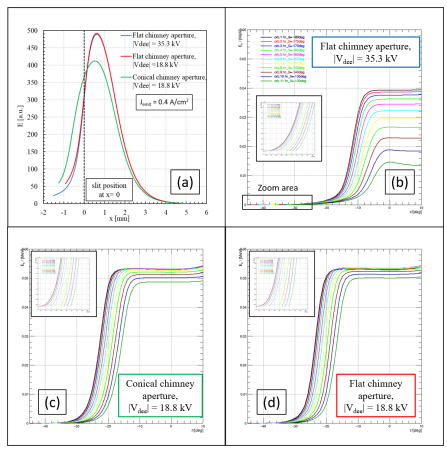

Figure 7: Electric field and energy gain in the first gap.

Space Charge in AOC

In the default use of AOC, the full 6D phase space of the initial particles in the bunch must be specified. Recently a new option has been added for simulating the formation of the bunch extacted from the ion source meniscus. In this case, the particle properties on the meniscus must be defined and also the number of time-steps that are needed to complete the bunch formation. The bunch will be sliced according to the number of time-steps. For each new step, the bunch is re-defined by adding the additional slice and then advanced using the iterative process. After completing the formation of the bunch, it is continued in the usual way.

FULL BEAM TRACKING

We track a full beam through the central region shown in Fig. 8. The position and orientation of the ion source and the first few accelerating gaps in this CR are optimized in order to obtain good beam centering and good vertical electric focusing. Some additional tools have been made in AOC that allow to slightly rotate/translate the central region geometry without the need to each time solve its 3D FEM model.

The collimators (shown in blue) are optimized to limit the accelerated RF phase range to about 40° and by so to remove particles that would otherwise be lost at higher energies. Note that the beam shown in Fig. 8 only includes the "succesfull" particles. The starting beam, obtained from a

ISBN: 978-3-95450-240-0 ISSN: 2673-5547 doi:10.18429/JACoW-HIAT2022-TUP17

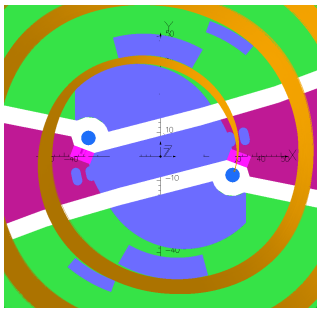

Figure 8: The 2-fold rotational symmetric central region.

SCALA simulation ($J_{emit} = 0.4$ A/cm^2 and $V_{dee} = 18.8$ kV) and representing a starting average current of 100 mA on the meniscus, is sampled with 100000 particles in a RF phase range between -180° and 0°. Figure 9 shows transmission (a), centering (b), vertical beam-size (c) and vertical emittance (d) of the accelerated beam during the first 25 turns. In the representation shown, the particles are binned according to their RF-starting phase on the meniscus in four groups of each 10° wide. Only particles in the phase range between -180° and -140° are accepted. The particles must leave early from the meniscus as explained before. Figure 9 (a) shows that there are high losses in the first 2 turns. This is not only due to the unfavorable transit time but also to the strong over-focusing action in the horizontal plane at the ion source exit (see Fig. 3). Only about 1.7% of the particles is accepted, corresponding to an average beam current of 1.7 mA.

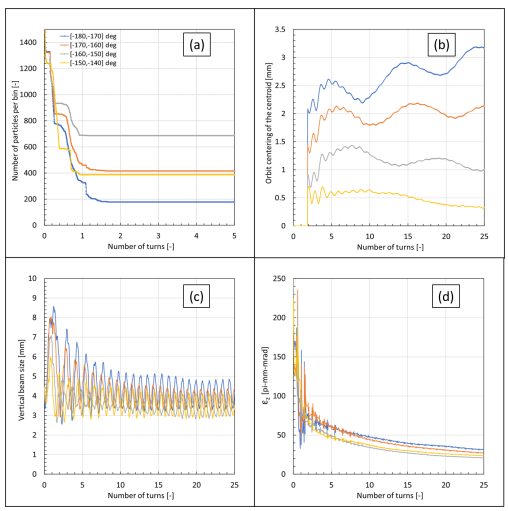

Figure 9: Beam rms properties, binned according to RF starting phase: (a) transmission, (b) beam centroid off-centering, (c) vertical beam size (2σ value), (d) normallized vertical emittance (2σ value).

The losses are distributed as follows: about 88.7% on the chimney+puller+puller collimators, about 5.8% in the phase selecting collimators and about 3.9% vertically on the dees and dummy dees. Beyond the 2nd turn all beam properties stabilize. Figure 10 (a) shows the shape of the accelerated bunches by their projection on the xy-plane, followed during 25 turns at moments when the RF phase equals zero. In another (earlier) simulation we started a bunch just beyond the source-puller gap with an average beam current of 5 mA, horizontal and vertical emittances of about 20 π·mm·mrad (1σ) and a total bunch length of about 3 mm (corresponding to 30° RF width). The shape of the bunches for this case is shown (for the first 20 turns) in Figure 10 (b). Here we observe the appearance of circular bunches (with a tail however) which probably is due to the well-known vortex motion [7], turned on by high space charge forces.

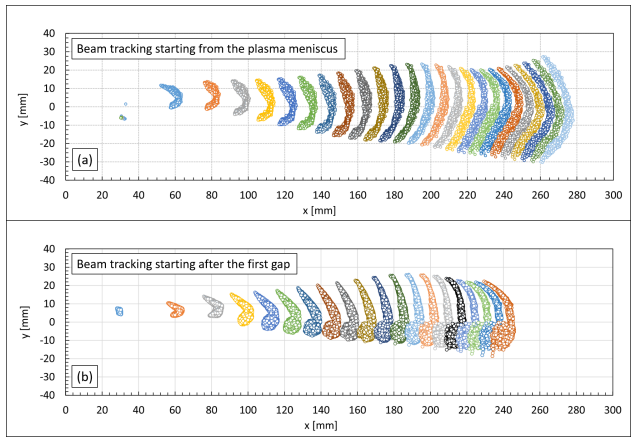

Figure 10: XY projection of accelerated bunches started (a) on the ion source meniscus and (b) after the first gap.

Optimization of Cyclotron Settings

Extracted beam optimization is a difficult and tedious process as it depends on multiple parameters (for example harmonic coil settings, dee-voltage, collimator geometry etc.) and requires full beam tracking (if possible with space charge) from the ion source up to the cyclotron exit. In order to facilitate this process an optimization program (`project_optimizer`) was written. This program uses standard optimization routines to optimize a task (project). The task is defined by a user-defined script which is executed by the program in an iterative process. It reads new values of independent variables as suggested by the program, executes the task and writes its results (new values of the objectives) to a file. The program then resumes and compares the results of the script with the (user defined) objectives in order to calculate the fitting error and suggest new values for the variables. This process is repeated until the fitting error is smaller than a given tolerance. In the present study, the script reads all AOC input data and adjust input field maps as needed. Then it runs AOC and post-process its results in order to extract the objective values. Three standard multiple dimension optimization routines have been implemented (Downhill Simplex Method, Direction SET Powell Method and Simulated Annealing Method) [8]).

The process has been tested (without space charge) for a beam of 2000 particles, tracked from the ion source position up to extraction. The starting conditions at the ion source were taken as: E = 100 eV, $\epsilon_x = 125\,\pi$·mm·mrad, $\epsilon_z = 500\,\pi$·mm·mrad, slit aperture $w \times h = 1 \times 4$ mm^2 and starting RF phases $-145° < \Phi < -115°$. The settings

ISBN: 978-3-95450-240-0 ISSN: 2673-5547 doi:10.18429/JACoW-HIAT2022-TUP17

of the two pairs of harmonic coils were optimized by `project_optimizer` to obtain maximum extraction efficiency on the first exit port. We found an extraction efficiency of 91% with 7.7% losses on the first beam separator and 1.3% extracted towards the 2nd exit port. Figure 11 illustrates the process of optimization of extraction efficiency as function of harmonic coil settings. Note that this case was still done "by hand".

Extraction efficiency [%] 1° exit port	Dee voltage 55.17 KV	Harmonic coils currents on the long poles					
		-0.35	-0.3	-0.25	-0.2	-0.15	-0.1
Harmonic coils current on the short poles	-0.35	59.2	63.1	68.5	76.0	78.7	78.4
	-0.3	59.8	67.0	78.4	82.1	82.2	81.1
	-0.25	60.9	77.2	87.7	87.9	84.9	84.3
	-0.2	81.8	89.6	89.4	89.2	83.7	69.0
	-0.15	91.3	87.3	82.2	68.5	52.3	45.7
	-0.1	76.9	66.3	65.0	72.5	67.6	12.6

Figure 11: Optimization of extraction efficiency.

Figure 12 (a,b) shows the extracted phase space just beyond the beam separator. At this point we find (1σ) emittances and energy spread of: $\epsilon_x = 104\,\pi$·mm·mrad, $\epsilon_z = 1.25\,\pi$·mm·mrad, $\Delta E/E = 0.44\%$. As can be seen, there is a large X vs Z asymmetry; the vertical emittance is nicely linear.

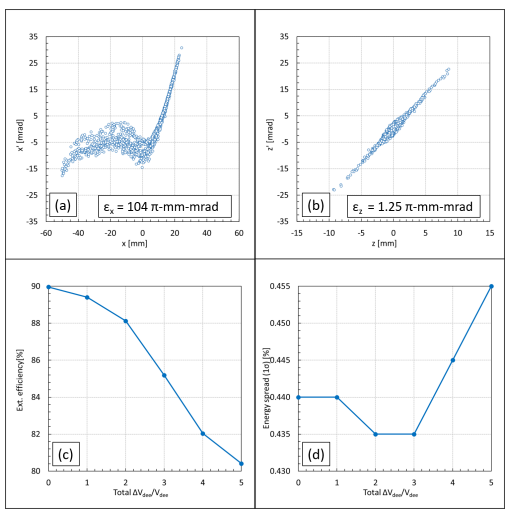

Figure 12: Extracted emittances and dependence of extraction efficiency and energy spread on dee-voltage ripple.

For the self-extracting cyclotron, good turn separation helps to obtain high extraction efficiency. Turn-separation may be reduced or lost if the RF dee-voltage is rippled. At high beam intensities this may happen due to beam loading of the RF cavity, if the injected beam intensity is noisy. Internal ion sources indeed are rather noisy. Figure 12 (c,d) shows the decrease of extraction efficiency and the beam energy spread as function of a simulated dee-voltage ripple. It is seen that the RF control system should keep this ripple as low as possible.

CONCLUSION

We developed new tools i) for the study of space charge beams extracted from the plasma meniscus and bunch formation in the source-puller gap and ii) for automated optimization of cyclotron settings aiming at highest extraction efficiency. Further studies are planned, to see if the turn-separation at extraction can be improved.

REFERENCES

[1] R. Alberto and H. Braband, "SPECT/PET Imaging with Technetium, Gallium, Copper, and Other Metallic Radionuclides", in *Comprehensive inorganic chemistry II: From elements to applications*, Amsterdam: Elsevier, pp. 785-817, 2013. doi:10.1016/B978-0-08-097774-4.00331-4

[2] W. Kleeven *et al.*, "The IBA self-extracting cyclotron project", in *Proc. Nukleonika*, vol. 48, pp. S59-S67, 2003.

[3] W. Kleeven, "Isochronous cyclotron and method of extraction of charged particles from such cyclotron", Patent No.: US 6,683,426 B1, Date: 27 January 2004

[4] G. D'Agostino *et al.*, "InnovaTron: An Innovative High-Intensity Industrial Cyclotron for Production of Tc-99m and Other Frontier Medical Radioisotopes", in *Proc. IPAC'21*, Campinas, Brazil, May 2021, pp. 1841–1844. doi:10.18429/JACoW-IPAC2021-TUPAB188

[5] OPERA, https://www.3ds.com/

[6] J. G. M. Kleeven *et al.*, "AOC, A Beam Dynamics Design Code for Medical and Industrial Accelerators at IBA", in *Proc. IPAC'16*, Busan, Korea, May 2016, pp. 1902–1904. doi:10.18429/JACoW-IPAC2016-TUPOY002

[7] J. G. M. Kleeven, "Some Examples of Recent Progress of Beam-Dynamics Studies for Cyclotrons", in *Proc. Cyclotrons'16*, Zürich, Switzerland, Sep. 2016, pp. 244–250. doi:10.18429/JACoW-Cyclotrons2016-WEA01

[8] William H. Press, Saul A. Teukolsky, William T. Vetterling, and Brian P. Flannery. "Numerical Recipes in C, The Art of Scientific Computing, Second Edition", Cambridge University Press, 1992. ISBN 0-521-43108-5.